Synthesis, Characterization, and Quantum-Chemical Studies of Ni(CN)₂MX (M = Rb, Cs; X = Cl, Br)

Xiaohui Liu,[†] Manfred Speldrich,[†] Paul Kögerler,[†] Richard Dronskowski,*,[†] and Andrei L. Tchougréeff[‡]

[†]*Institute of Inorganic Chemistry, RWTH Aachen University, Landoltweg 1, 52056 Aachen, Germany, and*
[‡]*Institute of Inorganic Chemistry, RWTH Aachen University, Landoltweg 1, 52056 Aachen, Germany, and Poncelet Laboratory, Independent University of Moscow, Moscow Center for Continuous Mathematical Education, Bolshoi Vlasevsky Per. 11, 119002 Moscow, Russia*

A new series of coordination-network compounds containing Ni(CN)₂ and MX (M = Rb, Cs; X = Cl, Br) quasi two-dimensional sheets has been synthesized and structurally characterized. The tetragonal crystal structure ($I4/mmm$, no. 139) can be derived from the distorted perovskite type. Chemically, the Lewis-acidic Ni(CN)₂ moieties accept halide ligands, resulting both in slightly elongated $[Ni(NC)_4X_2]^{4-}$ octahedra and strongly elongated $[Ni(CN)_4X_2]^{4-}$ octahedra that are charge-balanced by M^+ cations. Quantum-chemical calculations of the effective Hamiltonian crystal field (EHCF) type indicate the simultaneous presence of high- and low-spin Ni^{2+} in a 1:1 ratio, in agreement with GGA+U and UV studies reported here. Our magnetic susceptibility data also corroborate the theoretical findings. An analysis of the magnetic superexchange paths in the new series of compounds is performed as well as that of the tentative magnetic state of the series.

Introduction

Since the first occasion[1a] when solid-state cyanide-bridged coordination networks were obtained 300 years ago as Prussian blue species, the magnetic descendants of the compositions ($AM^{II}[M'^{III}(CN)_6]$) and $M_3^{II}[M'^{III}(CN)_6]_2$ originally reported in ref 1b have been widely investigated. This is because of their large diversity in terms of magnetic properties tunable by either magnetic fields, light, temperature, or pressure, but first of all by their composition.[2] Indeed, the cyanide anion remains one of the most commonly employed pseudohalide bridging ligands in the design of transition-metal complexes and networks. For example, flexible pillared or layered nickel cyanide networks with a linear bidentate ligand were recently investigated as interesting porous magnetic materials.[3] The structure of nickel cyanide Ni(CN)₂ was reported on the basis of X-ray and neutron powder diffraction, and the refinements evidenced Ni(CN)₂ as a sheet-like coordination polymer in which Ni

and cyanide ions form corner-sharing square-planar units, and the C and N atoms appear as being highly disordered,[4] at least from the crystallographic perspective. Nonetheless, C and N atoms are known to be well ordered in quasi-ternary coordination complexes between nickel cyanide and either ammonia,[5] benzene,[6] or ammonia with water[7] in structural voids, all of which were reported several decades ago. On the basis of the structural information of Ni(CN)₂NH₃, a new series of nickel cyanide solid-state phases of the general composition Ni(CN)₂MX (M = Rb, Cs; X = Cl, Br) where the Lewis-acidic Ni(CN)₂ moieties accept halide ligands, resulting in $[Ni(NC)_4X_2]^{4-}$ and $[Ni(CN)_4X_2]^{4-}$ octahedra that are charge-balanced by M^+ cations, has been designed. Herein, we report the synthesis, structure, and quantum-chemical and magnetic studies of the four compounds Ni(CN)₂RbCl (**1**), Ni(CN)₂CsCl (**2**), Ni(CN)₂RbBr (**3**), and Ni(CN)₂CsBr (**4**).

Experimental Section

All chemicals were purchased from Sigma-Aldrich and used as received. Most experimental steps were either performed under argon using standard Schlenk techniques or directly in an argon-filled glovebox. The mixed salts MX/LiX as reactants and fluxes (RbCl/LiCl: 41.5/58.5 mol percent;

*To whom correspondence should be addressed. E-mail: drons@ HAL9000.ac.rwth-aachen.de.

(1) (a) Anonymous. *Miscellanea Berolinensia ad Incrementum Scientiarum* **1710**, *1*, 377. (b) Ferlay, S.; Mallah, T.; Ouahès, R.; Veillet, P.; Verdaguer, M. *Nature* **1995**, *378*, 701.

(2) (a) Miller, J. S. *Inorg. Chem.* **2000**, *39*, 4392. (b) Entley, W.; Treadway, C. R.; Girolami, G. S. *Mol. Cryst. Liq. Cryst.* **1995**, *273*, 153. (c) Miller, J. S.; Drillon, M. *Magnetism: Molecules to Materials*; Wiley-VCH: Weinheim, Germany, 2002.
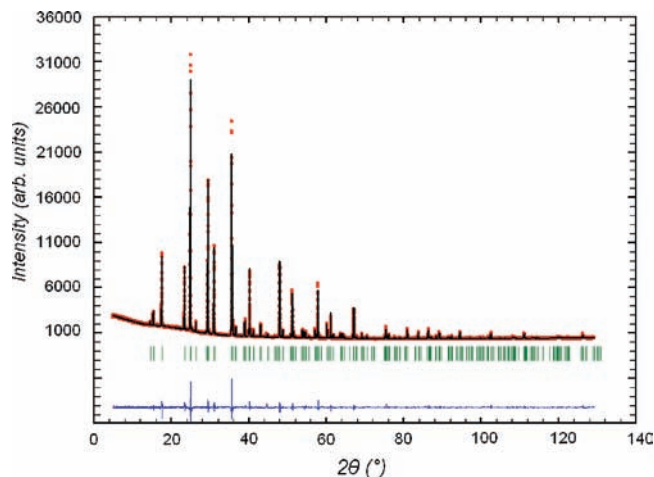
(3) Culp, J. T.; Smith, M. R.; Bittner, E.; Bockrath, B. *J. Am. Chem. Soc.* **2008**, *130*, 12427.

(4) Hibble, S. J.; Chippindale, A. M.; Pohl, A.; Hannon, A. C. *Angew. Chem., Int. Ed.* **2007**, *46*, 7116.

(5) Rae, A. I. M.; Maslen, E. N. *Z. Kristallogr.* **1966**, *123*, 391.

(6) Rayner, J. H.; Powell, H. M. *J. Chem. Soc.* **1952**, 319.

(7) Rayner, J. H.; Powell, H. M. *J. Chem. Soc.* **1958**, 3412.

Figure 1. Observed, calculated, and difference intensities for the X-ray Rietveld refinement of $Ni(CN)_2RbBr$. The vertical markers show the positions of the Bragg reflections.

eutectic temperature 314 °C; CsCl/LiCl: 40.5/59.5, 306 °C; RbBr/LiBr: 46.0/54.0, 300 °C; CsBr/LiBr: 50.0/50.0, 313 °C) were heated to 550 °C until they were melted and vapor-free, then were evacuated immediately in the small chamber of the glovebox and kept in the argon-filled glovebox. The starting phase $Ni(CN)_2NH_3$ was prepared by adding a large excess of 7.0 M ammonia solution to a 0.1 M aqueous solution of $K_2[Ni(CN)_4]$ and $NiCl_2 \cdot 6H_2O$ until a clear blue solution was formed, which was stirred overnight. The resulting precipitate was subsequently filtered, washed well with water, and dried in the air. Purity was verified by CHN elemental analysis. Bulk $Ni(CN)_2NH_3$ always contains small residues of water, but the exact amount strongly depends on the reaction condition despite the fact that single crystals are of good quality in all cases. Residual H_2O contained in $Ni(CN)_2NH_3$ has, however, no influence on the subsequent reaction (see below). The purity of the products **1**−**4** was checked by CHN and AAS analysis and X-ray powder diffraction as well as by IR spectroscopy.

$Ni(CN)_2RbCl$ (**1**) was prepared by a typical solid−liquid reaction involving a mixture of 1.0 mmol of $Ni(CN)_2NH_3$ and 6.0 mmol of RbCl/LiCl as reactive salts in a long Schlenk glass under a vacuum. The mixture was first heated at 250 °C under a vacuum overnight to remove traces of H_2O and NH_3, accompanied by a color change from blue to green-yellow. The Schlenk glass was filled with pure argon, heated to 360 °C for 10 h, and then allowed to cool to room temperature. Well-crystallized products were obtained, washed with water, filtered, and air-dried. Yield: 90%. Anal. Calcd for $Ni(CN)_2$-RbCl: C, 10.37; H, 0; N, 12.09; Ni, 25.34; Rb, 36.90. Found: C, 10.20; H, 0.12; N, 12.01; Ni, 25.20; Rb, 36.95. IR spectrum (KBr, cm^{-1}): 2165 (s), 452 (m). Single-crystal X-ray diffraction: chemical formula C_2ClN_2NiRb, $M = 231.65$, tetragonal $I4/mmm$, $a = b = 7.1209(10)$ Å, $c = 11.008(2)$ Å, $V = 558.19(16)$ Å^3, $Z = 4$, $F(000) = 432$, $S = 1.05$, 2066 reflections measured, 272 unique, final $R_1 = 0.035$, $wR_2 = 0.096$ for 170 observed reflections and $I > 2\sigma(I)$.

$Ni(CN)_2CsCl$ (**2**), and $Ni(CN)_2RbBr$ (**3**), and $Ni(CN)_2$-CsBr (**4**) were prepared following the procedure described for $Ni(CN)_2RbCl$. Yield: 93%. Anal. calcd for $Ni(CN)_2CsCl$: C, 8.61; H, 0; N, 10.04; Ni, 21.03; Cs, 47.62. Found: C, 8.60; H, 0.10; N, 10.10; Ni, 21.05; Cs, 47.53. IR spectrum (KBr, cm^{-1}): 2160 (s), 446 (m).

Compound **3**. The result of the final Rietveld refinement of $Ni(CN)_2RbBr$ is shown in Figure 1. Yield: 92%. Anal. Calcd for $Ni(CN)_2RbBr$: C, 8.70; H, 0; N, 10.15; Ni, 21.26; Rb, 30.96. Found: C, 8.72; H, 0.07; N, 10.20; Ni, 21.19; Rb, 31.01. IR spectrum (KBr, cm^{-1}): 2169 (s), 450 (m).

Compound **4**. Yield: 95%. Anal. Calcd for $Ni(CN)_2CsBr$: C, 7.42; H, 0; N, 8.66; Ni, 18.14; Cs, 41.08. Found: C, 7.40; H, 0.05; N, 8.64; Ni, 18.16; Cs, 41.10. IR spectrum (KBr, cm^{-1}): 2155 (s), 443 (m). Single-crystal X-ray diffraction: chemical formula C_2BrCsN_2Ni, $M = 323.57$, tetragonal $I4/mmm$, $a = b = 7.1704(3)$ Å, $c = 11.4149(12)$ Å, $V = 586.89(7)$ Å^3, $Z = 4$, $F(000) = 576$, $S = 1.22$, 2331 reflections measured, 291 unique, final $R_1 = 0.053$, $wR_2 = 0.126$ for 256 observed reflections and $I > 2\sigma(I)$.

X-Ray Crystallography. Single-crystal data were collected at 293(2) K using a Bruker SMART APEX CCD diffractometer with graphite-monochromatized Mo Kα radiation. An empirical absorption correction was performed with SADABS. The structures were solved by direct methods and refined by full-matrix least-squares techniques based on intensities with the SHELX program package.[8] During the structure refinements, the exchanged position and mixed occupation of C and N were considered, but the results were inferior. We believe that C and N are well ordered in the crystals (see structure discussion) on the basis of crystallographic data and also chemical reasons.

The X-ray powder diffraction data were recorded at room temperature by means of a calibrated STOE STADI MP powder diffractometer in transmission geometry with strictly mono-chromatized Cu Kα$_1$ radiation and a linear position-sensitive detector (PSD) with a flat sample holder; the range of measurement was a very wide 5−130° in 2Θ with individual steps of 0.01°. The X-ray powder diagrams of **1**−**4** were indexed using tetragonal unit cells and $I4/mmm$ space-group symmetry. The primary structural model (atomic positions) came from single-crystal results. The FULLPROF program package[9] was used for the Rietveld refinement with a pseudo-Voigt profile function, and the backgrounds of the data sets were manually subtracted by linear interpolation. Anisotropic displacement parameters for all metal and halide atoms were used as well as isotropic displacement parameters for C and N atoms. Tables 1 and 2 contain all important crystallographic data and intera-tomic distances. Additional structural details may be obtained from FIZ Karlsruhe, D-76344 Eggenstein-Leopoldshafen, on quoting the depository numbers CSD-380471 for **1**, CSD-380469 for **2**, CSD-380470 for **3**, and CSD-380468 for **4**.

Spectroscopic Measurements. FT-IR spectra were recorded on a Nicolet 6700 spectrometer using KBr pellets in the region 400−4000 cm^{-1}. Solid-state UV/vis spectra were measured in the reflection mode with a J&M Tidas (Zeiss Axioplan 2) Heraeus spectrometer.

Magnetic Measurements. The temperature-dependent magnetic susceptibilities of **1** and **2** were determined by SQUID magnetometry (Quantum Design MPMS 5XL) between 2 and 300 K in an applied field of 0.5 T. The data were corrected for sample holder (PTFE capsules) and diamagnetic contributions of Ni^{2+} and the ligands (calculated from tabulated values; $\chi_m^{dia} = -119 \times 10^{-11}$ m^3 mol^{-1} for both compounds).[10,11]

Theory

Effective Hamiltonian Crystal Field (EHCF) Theory. The quantum-chemical study of a structural cut from the extended crystal structure of **1** was performed using the effective Hamiltonian crystal field (EHCF) method,[12] which attributes the observed splitting dominantly to the contribution of the one-electron transfers between the d shells (partially) filled by an integer number of

(8) Sheldrick, G. M. *Acta Crystallogr.* **2008**, *A64*, 112.
(9) Rodriguez-Carvajal, J. *Fullprof2000*, version 3.2; Laboratoire Léon Brillouin: Gif-sur-Yvette Cedex, France, 1997.
(10) Haberditzl, W. *Angew. Chem.* **1966**, *78*, 277.
(11) Lueken, H. *Magnetochemie*; Teubner: Stuttgart, Germany, 1999.
(12) Soudackov, A. V.; Tchougréeff, A. L.; Misurkin, I. A *Theor. Chim. Acta* **1992**, *83*, 389.

Table 1. Crystal Data of $Ni(CN)_2MX$ from Rietveld Refinements of X-Ray Powder Diffraction Measurements

	$Ni(CN)_2RbCl$ (**1**)	$Ni(CN)_2CsCl$ (**2**)	$Ni(CN)_2RbBr$ (**3**)	$Ni(CN)_2CsBr$ (**4**)
molar mass	231.67 g/mol	279.09 g/mol	276.12 g/mol	323.57 g/mol
color and form	green microcrystals	green microcrystals	green microcrystals	green microcrystals
lattice parameters	$a = b = 7.10850(7)$ Å	$a = b = 7.15076(5)$ Å	$a = b = 7.11841(5)$ Å	$a = b = 7.17111(5)$ Å
	$c = 10.92901(12)$ Å	$c = 11.0199(10)$ Å	$c = 11.50366(13)$ Å	$c = 11.50907(10)$ Å
cell volume	552.252(10) Å^3	563.484(8) Å^3	582.922(9) Å^3	591.852(7) Å^3
space group; Z	$I4/mmm$ (no. 139); 4	$I4/mmm$ (no. 139); 4	$I4/mmm$ (no. 139); 4	$I4/mmm$ (no. 139); 4
no. of reflns	108 ($2\theta = 6-100°$)	169 ($2\theta = 5-129°$)	173 ($2\theta = 5-129°$)	173 ($2\theta = 5-129°$)
R_p, R_{wp}, R_{Bragg}	0.032, 0.048, 0.026	0.035, 0.048, 0.031	0.039, 0.057, 0.036	0.042, 0.060, 0.037

Table 2. Selected Bond Lengths (Å) in $Ni(CN)_2MX$

	$Ni(CN)_2RbCl$	$Ni(CN)_2CsCl$	$Ni(CN)_2RbBr$	$Ni(CN)_2CsBr$
Ni1−X	3.013(2)	3.050(3)	3.1351(12)	3.1549(15)
Ni2−X	2.451(2)	2.460(3)	2.6168(12)	2.5997(15)
Ni1−C	1.8518(1)	1.874(8)	1.857(5)	1.893(6)
Ni2−N	2.0287(1)	2.059(6)	2.046(4)	2.053(4)
C−N	1.1460(1)	1.124(10)	1.131(6)	1.125(7)

electrons and both occupied and vacant ligand MOs. This is reached by assuming the many-electron wave function of a transition metal compound to have the form

$$\Psi_n = \Phi_d^{(n)} \times \Phi_l$$

where $\Phi_d^{(n)}$ is the nth full configuration-interaction function of n_d electrons in the d-shell of the transition-metal ion and Φ_l is the function of all other (n_l) electrons of the system taken in a semiempirical self-consistent field approximation; the product sign $\times$ indicates that the resulting function is antisymmetric (i.e., changes its sign) when the coordinates of each pair of n_d+n_l electrons are interchanged. This type of wave function formalizes the usual assumptions of the crystal field theory.[13,14] It is approximate because the Hamiltonian of the transition-metal complex always contains resonance terms, responsible for one-electron transfers between the d shell and the rest of the complex molecule. The effective Hamiltonian for the d shell has the following form:

$$H_d^{eff} = H_{lf} + H_{ee}$$

H_{lf} stands for the one-electron operator describing interactions of the electrons in the d shell with the atomic core of the transition-metal ion and the entire surrounding area. H_{ee} is the two-electron operator describing the Coulomb interactions between the d electrons. The symmetry properties H_d^{eff} are those of Bethe's crystal field theory. The matrix elements of its one-electron contribution H_{lf} are not taken as parameters but, by contrast, are calculated within the EHCF procedure.

In the solid-state context, the EHCF method has been employed in its cluster version[15−17] in which the d chromophores of interest are supplied by ligand spheres

represented by structural cuts taken from the crystal. In the present study, we employed two cluster models each containing 11 atoms, that is, one Ni^{2+} ion, two Cl^- ions, and four CN^- groups with an overall cluster charge of -4. Two types of clusters were used in order to model the Ni^{2+} ions coordinated by the CN^- groups in the cyanide or nitrile manner as occurring in the material.

Correlated Density-Functional Theory. Alternative density-functional calculations including explicit electronic correlation (of the GGA+U type) were performed using plane waves and pseudopotentials by means of the computer program VASP (Vienna *Ab Initio* Simulation Package)[18,19] employing the generalized-gradient approximation (GGA) of the PBE type[20] and the projected-augmented wave (PAW) method.[21] The cutoff energy was set to 500 eV. The correlation is taken into account following the scheme[22] with the parameters U and J expressed through the Slater−Condon parameters F^k for the d shells according to[23]

$$U_{Ni} = \alpha F_{Ni}^0, \quad J_{Ni} = \alpha \frac{13}{112} F_{Ni}^2$$

The empirical values of the F^k parameters taken from ref 12 had been scaled uniformly by the factor $\alpha = 0.4$ following ref 23, resulting in the parameters $U = 7.074$ eV and $J = 0.6075$ eV for nickel, which seem to be reasonable values, close to those normally used in the GGA+U context.

Results and Discussion

Synthesis and Crystal Structure. The synthesis of $Ni(CN)_2MX$ occurs by a two-step reaction. First, NH_3 is removed from $Ni(CN)_2NH_3$ by heating to form badly crystallized $Ni(CN)_2$ in *statu nascendi*, immediately followed by an acid−base reaction at 300 °C in which the Lewis-acidic $Ni(CN)_2$ moieties accept halide ligands from MX to result in $Ni(CN)_2MX$.

The four $Ni(CN)_2MX$ (M = Rb, Cs; X = Cl, Br) compounds are iso-structural. For a better comparison, we list their crystallographic data on the basis of the powder XRD refinements in Table 1. The crystal structure can

(13) Bethe, H. A. *Ann. Phys.* **1929**, *395*, 133.
(14) Lever, A. B. P. In *Inorganic Electronic Spectroscopy*; Elsevier: Amsterdam, 1984; pp 317−333.
(15) Tchougréeff, A. L. *J. Mol. Catal.* **1997**, *119*, 377. Razumov, M. G.; Tchougréeff, A. L. *Zh. Fiz. Khim.* **2000**, *74*, 87. [*Russ. J. Phys. Chem.* **2000**, *74*, 78].
(16) Tokmachev, A. M.; Tchougréeff., A. L. *J. Sol. State Chem.* **2003**, *176*, 633.
(17) Liu, X.-H.; Dronskowski, R.; Glaum, R.; Tchougréeff, A. L. *Z. Allg. Anorg. Chem.* **2010**, *636*, 343.

(18) Kresse, G.; Furthmüller, J. *Comput. Mater. Sci.* **1996**, *6*, 15. Kresse, G.; Furthmüller, J. *Phys. Rev. B* **1996**, *55*, 11169.
(19) Kresse, G.; Hafner, J. *Phys. Rev. B* **1993**, *47*, 558–561. Kresse, G.; Hafner, J. *Phys. Rev. B* **1994**, *49*, 14251.
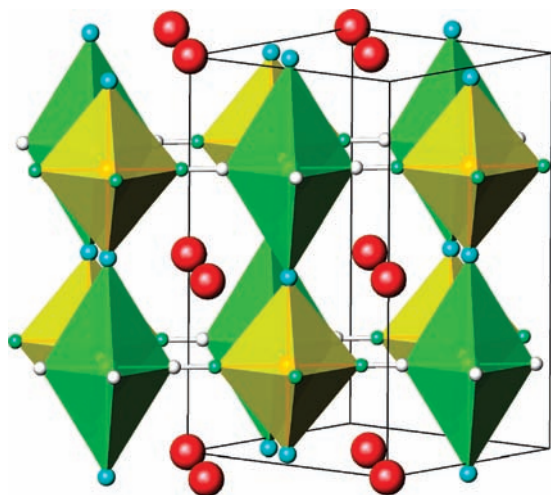(20) Perdew, J. P.; Burke, K.; Ernzerhof, M. *Phys. Rev. Lett.* **1996**, *77*, 3865.
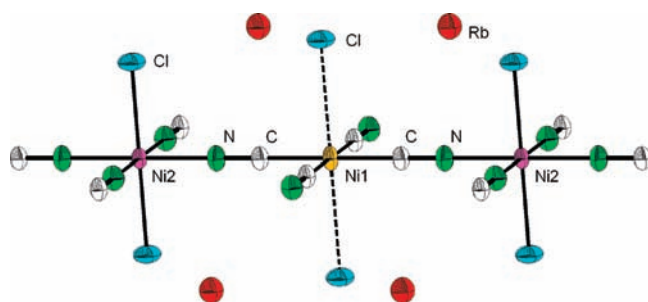(21) Blöchl, P. E. *Phys. Rev. B* **1994**, *50*, 17953.
(22) Dudarev, S. L.; Botton, G. A.; Savrasov, S. Y.; Humphreys, C. J.; Sutton, A. P. *Phys. Rev. B* **1998**, *57*, 1505.
(23) Tchougréeff, A. L.; Dronskowski, R. *J. Comput. Chem.* **2008**, *29*, 2220.
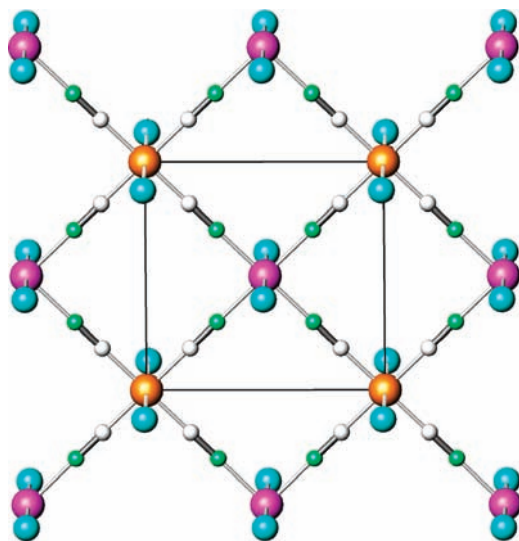
Figure 2. Crystal structure of Ni(CN)$_2$MX (M = Rb, Cs; X = Cl, Br) showing green octahedra around Ni1 (four white C and two blue Cl atoms) and yellow octahedra around Ni2 (four green N and two blue Cl atoms).

Figure 3. ORTEP representation of **1** with thermal ellipsoids corresponding to 90% probability based on the refined structure using single-crystal data. The ions in the orange Ni1 positions are the cyanide coordinated low-spin (ls) ions, whereas those in the magenta Ni2 positions are the nitrile coordinated high-spin (hs) ones.

Figure 4. View into the *ab* plane of the crystal structure of Ni(CN)$_2$MX (M = Rb, Cs; X = Cl, Br) in which the Ni(CN)$_2$ units generate a two-dimensional network. Ni1 in orange, Ni2 in magenta, X in blue, N in green, and C in white. The M$^+$ ions have been omitted for clarity.

be imagined as being of the distorted perovskite type and is best described in the tetragonal space group *I*4/*mmm* (no. 139). It comprises distorted $[Ni(NC)_4X_2]^{4-}$ and $[Ni(CN)_4X_2]^{4-}$ octahedra (both elongated), which are charge-balanced by M$^+$ cations located in the voids (Figure 2).

The connectivity mode of **1** is visualized in Figure 3 together with thermal ellipsoids. The Ni1 atoms form more strongly distorted octahedra in which one finds four cyanide C atoms in the basal plane and two halide anions as top/bottom atoms. The Ni1−C bond lengths range from 1.852 to 1.893 Å, depending on M and X, while the Ni1−X bond lengths are 3.03 ± 0.02 Å for Cl$^-$ and 3.14 ± 0.01 Å for Br$^-$. The Ni2 atoms are those with the nitrile coordination of the CN$^-$ groups forming somewhat less distorted octahedra with four N atoms in the basal plane and two halide anions as top/bottom atoms. The Ni2−N bond lengths range from 2.029 to 2.059 Å, depending on M and X as seen previously, while the Ni2−X bond lengths fall in the range of 2.45 ± 0.01 Å for Cl$^-$ and 2.60 ± 0.02 Å for Br$^-$. It is clear that the Ni1−X distances (cyanide coordination) are a little longer than the sum of the effective ionic radii (Ni^{2+}, 0.69; Cl$^-$, 1.81; Br$^-$, 1.96 Å). By contrast, the Ni2−X distances are slightly shorter than the sum of the respective ionic radii. The different strengths of the ligand fields are also quite predictable by comparing the differences in octahedral dis-

tortions for the weak ligand-field site $[Ni(NC)_4X_2]^{4-}$ and the strong ligand-field site $[Ni(CN)_4X_2]^{4-}$ (see below).

In the crystal, the Ni(CN)$_2$ units generate a planar layered structure (Figure 4) in which each layer consists of alternating Ni^{2+} and CN$^-$ ions, somewhat similar to the situation in the aforementioned compounds between nickel cyanide and ammonia, water, and benzene.[5−7] Consequently, the length of the *a* axis of Ni(CN)$_2$MX is almost identical with the one of Ni(CN)$_2$NH$_3$. We conclude that the Ni−C−N−Ni vector coincides with the diagonal of the *ab* plane of the unit cell, and the nickel and cyanide ions are bonded to yield an extended square array similar to all Ni(CN)$_2$ derivatives. Nonetheless, the Ni−Ni distance in the present layer (ca. 5.03 Å) is longer than that in pure Ni(CN)$_2$ (4.86 Å); the latter has been described as being disordered in terms of C and N positions.[4] The behavior of the lattice parameters of **1** as a function of the temperature was studied between 4 and 300 K by X-ray diffraction, but no negative thermal expansion (NTE) has been observed, in contrast to the two-dimensional NTE that was reported for Ni(CN)$_2$,[4] and anomalous zero thermal expansion reported in ref 24 for Fe[Co(CN)$_6$].

In the ideal Prussian blue (AM^{II}[M$'^{III}$(CN)$_6$]) structure or in its descendant M$_3^{II}$[M$'^{III}$(CN)$_6$]$_2$, which became a prototypic compound for many three-dimensional magnets (see below) as departing from that with M = V and M$'$ = Cr (with certain nonstoichiometry),[1b] there are linear M−CN−M$'$ bridges which form a three-dimensional network. In comparison, the Ni(CN)$_2$MX structure may be considered either as a less densely packed three-dimensional network or even as a quasi two-dimensional one since the interlayer interactions can be thought to be considerably weaker as mediated by the halogen anions. The latter description would enormously aid in making the magnetic properties more transparent

(24) Margadonna, S.; Prassides, K.; Fitch, A. N. *J. Am. Chem. Soc.* **2004,** *126*, 15390.

and easier to understand. In addition, the analogues of Prussian blue exhibit, in many cases, defect structures such that the magnetic properties are influenced by site vacancies. The perfectly ordered crystals of $Ni(CN)_2MX$, however, offer the possibility to study the magnetic properties in detail.

Quantum-Chemical Study (EHCF). The EHCF calculations for the $[Ni(CN)_4Cl_2]^{4-}$ and $[Ni(NC)_4Cl_2]^{4-}$ clusters cut from the crystal structure of **1** are easy to understand. Given the local structure, the cyanide cluster $[Ni(CN)_4Cl_2]^{4-}$ has a low-spin (ls: $S = 0$) ground state with an electronic configuration of $e^4a_1{}^2b_2{}^2$, whereas the nitrile cluster $[Ni(NC)_4Cl_2]^{4-}$ has a high-spin one (hs: $S = 1$) with the electronic configuration $b_1{}^2e^4a_1{}^1b_2{}^1$. [The labels of the one-electron states (irreducible representations of the C_{4v} point group of the cluster) refer to the actual situation in the crystal where the cyanide groups are oriented along the diagonals of the coordinate system and where the x and y axes are parallel to the crystallographic a and b directions such that the lobes of the doubly occupied b_1 orbital ($d_{x^2-y^2}$) point to the void space between the cyanide groups whereas those of the b_2 orbital (d_{xy}) point to their lone pairs (see Figures 2 and 4).] The choice of the coordinate system results in an energetic interchange of the orbital order ($\varepsilon(b_1) < \varepsilon(b_2)$) on the energy scale, opposite to that under the traditional choice of the coordinate axes (cyanide/nitrile groups along the x and y axes). This manifests itself in the negative sign of the spectrochemical Dq parameter which is defined by $10Dq = \varepsilon(b_1) - \varepsilon(b_2)$.[11,14] For the ls Ni1 atom (cyanide mode of coordination), the following splitting parameters of the d shell are obtained: $Dq = -3003$ cm^{-1}, $Ds = 2223$ cm^{-1}, $Dt = -1757$ cm^{-1}, to be compared with the analogous parameters of the hs Ni2 atom (nitrile mode of coordination): $Dq = -1380$ cm^{-1}, $Ds = 474$ cm^{-1}, $Dt = -1083$ cm^{-1}. This results in more than a 2-fold decrease of the absolute value of the principal splitting parameter Dq when going from the cyanide-coordinated to the nitrile-coordinated Ni^{2+} ion, more than a 4-fold decrease of the Ds parameter and a somewhat less pronounced decrease of the absolute value of the Dt parameter. Thus, all the d-shell splitting parameters are significantly smaller for the nitrile-coordinated hs Ni2 ion than for the cyanide-coordinated ls Ni1 ion.

The EHCF method generally serves to solve the direct spectral problem for the open d shells in the arbitrary effective crystal field. When supplied by the Racah parameters B and C describing the Coulomb interactions, it can provide predictions of the spectra of the intrashell d–d excitations. In the present materials, with two types (ls and hs) of Ni^{2+} ions, one should expect two types of the spectra originating, respectively, from the singlet (ls) and triplet (hs) ground states of the Ni^{2+} ions stipulated by the high-field cyanide and low-field nitrile coordination pattern. The results of the spectra calculations performed with the Racah parameters $B = 783$ cm^{-1} and $C = 3687$ cm^{-1} [25] as characteristic values for a series of Ni^{2+} complexes and with the two sets of the effective crystal field parameters calculated above for the two coordination patters (cyanide and nitrile) are given in Tables 3 and 4,

Table 3. Predicted Spectrum of the ls Ni^{2+} (Cyanide-Coordinated) Ion in $RbNi(CN)_2Cl$

transition	E (eV)	E (cm^{-1})	λ (nm)
$^1A_1 \rightarrow {}^3B_2$	1.42	11497	880
$^1A_1 \rightarrow {}^3E$	1.72	13924	727
$^1A_1 \rightarrow {}^3A_2$	2.45	19815	510
$^1A_1 \rightarrow {}^1B_2$	3.08	24909	405
$^1A_1 \rightarrow {}^1E$	3.26	26330	383
$^1A_1 \rightarrow {}^1A_2$	3.47	28051	360

Table 4. Predicted Spectrum of the hs Ni^{2+} (Nitrile-Coordinated) Ion in $RbNi(CN)_2Cl$

transition	E (eV)	E (cm^{-1})	λ (nm)
$^3B_2 \rightarrow {}^3E$	0.97	7891	1289
$^3B_2 \rightarrow {}^1A_1$	1.23	9953	1016
$^3B_2 \rightarrow {}^1B_2$	1.64	13299	762
$^3B_2 \rightarrow {}^3B_1$	1.71	13799	730
$^3B_2 \rightarrow {}^3A_2$	1.73	13971	722
$^3B_2 \rightarrow {}^3E$	2.22	17966	563
$^3B_2 \rightarrow {}^1E$	2.56	20672	488
$^3B_2 \rightarrow {}^1A_2$	2.95	23807	424
$^3B_2 \rightarrow {}^1A_1$	3.11	25133	401
$^3B_2 \rightarrow {}^3A_2$	3.14	25400	398
$^3B_2 \rightarrow {}^1B_1$	3.29	26566	380
$^3B_2 \rightarrow {}^3E$	3.37	27189	371
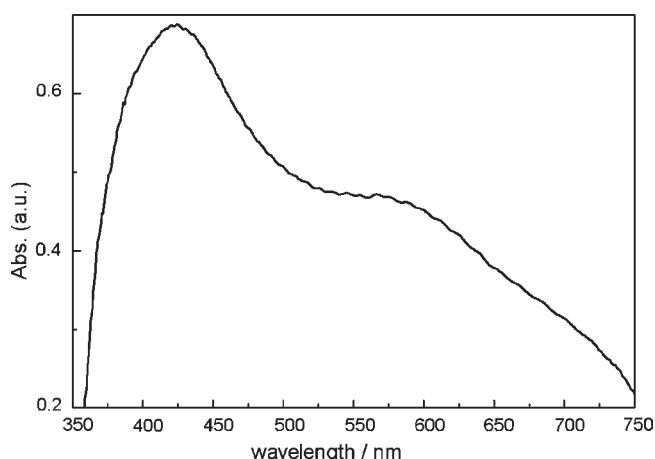
Figure 5. UV–vis spectrum of $Ni(CN)_2RbCl$.

respectively. While comparing the predicted spectrum with the experimental one given in Figure 5, one immediately realizes the low experimental resolution: the number of observed lines is much smaller than that of the theoretically predicted spin-allowed transitions. The somewhat asymmetric form of the most intense absorption line at 390–460 nm suggests that it is convoluted from several individual absorption lines. The same applies to other features that can be seen in the experimental spectrum. With this assumption, the agreement among the values calculated within the direct spectral problem formulation and the experimental data is satisfactory. Indeed, the strong wide line with the maximum at *ca.* 440 nm can be attributed to the spin-allowed transitions, namely, $^1A_1 \rightarrow {}^1B_2$, $^1A_1 \rightarrow {}^1E$, and $^1A_1 \rightarrow {}^1A_2$ in the d shells of the ls Ni^{2+} ions, which are predicted at 405, 383, and 360 nm, respectively. These values show some red-shift as compared to the ZINDO results obtained in ref 26 for

(25) Soudackov, A. V.; Tchougréeff, A. L.; Misurkin, I. A *Int. J. Quantum Chem.* **1996**, *58*, 161. *Int. J. Quantum Chem.* **1996**, *57*, 663.

(26) Mantz, Y. A.; Musselman, R. L. *Inorg. Chem.* **2002**, *41*, 5770.

the isolated $[Ni(CN)_4]^{2-}$ (cyanide coordination) ion. This broad asymmetric line can also be contributed by the allowed transitions $^3B_2 \rightarrow {}^3A_2$ and $^3B_2 \rightarrow {}^3E$ stemming from the hs Ni^{2+} ions predicted at 398 and 371 nm, respectively. A weaker feature in the measured spectrum at ca. 570 nm then must be attributed to the spin-allowed $^3B_2 \rightarrow {}^3E$ transition predicted at 563 nm as stemming from the hs Ni^{2+} ions. Although the intensity of this transition is ca. 3.5 times lower than that of the intense line at ca. 440 nm, it is still an allowed transition. We do not expect that any of the predicted spin-forbidden transitions can be seen on the same graph because of the large difference in intensities compared with the allowed transitions. The predicted lowest-energy allowed $^3B_2 \rightarrow {}^3E$ transition stemming from the hs Ni^{2+}, however, cannot be seen in the measured spectra since it must appear at ca. 1250 nm, beyond the long wave border (750 nm) of our measurements.

Density-Functional Theory (GGA+U). The GGA+U study on **1** using periodic boundary conditions was performed for three initial distributions of magnetic momenta: one corresponding to the opposite orientation of the $S = 1$ spins in two neighboring nitrile-coordinated Ni^{2+} ions, referred to hereafter as AF0; one for an antiferromagnetic arrangement of the $S = 1/2$ spins in all Ni^{2+} ions, referred to hereafter as AF1; and one for a ferromagnetic arrangement of the $S = 1$ spins in two neighboring nitrile-coordinated Ni^{2+} ions, referred to hereafter as FM. The AF1 and FM initial states both converge to the same ferromagnetic state in which only the nitrile-coordinated Ni ions bear noticeable spin density, as expected. The AF0 initial state converges to an antiferromagnetic state. In all three cases, the band gap amounts to ca. 2.6 eV, with the states at the top of the valence band composed of the Ni d states somewhat hybridized with the Cl, N, and C states. The values of the band gap are significantly larger than those reported in ref 27 for the $CsNi[Cr(CN)_6]$ three-dimensional representative of the Prussian blue magnets' family. The magnetic moments are in agreement with the EHCF findings: half of the Ni ions, namely, the nitrile-coordinated ones, are hs; they contain 1.773 unpaired electrons in the d shell each, either for the antiferromagnetic or for the ferromagnetic ground state. This is considerably larger than the value reported in ref 27 for the $CsNi[Cr(CN)_6]$ but somewhat lower than the values reported in ref 28 for $KNi[Cr(CN)_6]$ and fairly coincides with the analogous value reported in ref 29. The other half of the Ni^{2+} ions, the cyanide-coordinated ones, are of the ls type and consistently do not bear any noticeable spin density.

The total spin polarization, not just in the d shell but integrated over the unit cell obtained in the present GGA+U study, is almost ideal because the total amount of unpaired electrons with one of the spin projections per hs Ni^{2+} ion is 1.97, to be compared with the theoretical value of 2. The energy difference between the ferromagnetic and antiferromagnetic states is meager and amounts to only 0.2 meV, which basically is only twice as large as

the convergence criterion used throughout the calculation. Thus, on the basis of these data, it is *not* possible to say which of the spin arrangements is in fact predicted to be the ground state, but they may serve as estimates of the effective magnitude of the exchange (see below).

Magnetic Properties. The magnetochemical description of **1** and **2** using low-field susceptibility data is based on the phenomenological molecular-field approach due to the presence of a multitude of possible distinct exchange pathways as well as the different local coordination environments. On the basis of the electronic configuration ($3d^8$) of a Ni^{2+} center in a tetragonally distorted octahedral coordination environment and the resulting orbital singlet term $^3B_2$, Curie-type spin magnetism (i.e., temperature independence of μ_{eff}) is expected if exchange interactions and saturation effects are assumed to be insignificant. However, three factors cause the observed deviations from this scenario: (1) orbital momentum contributions, (2) antiferromagnetic coupling between hs Ni^{2+} sites within a given $Ni(CN)_2$ layer, and (3) weaker antiferromagnetic interactions between hs Ni^{2+} spin sites of adjacent layers.

The magnetic data were analyzed using the program CONDON[30] using a complete basis set (full d manifolds, i.e., 45 functions for Ni^{2+}) as a function of the applied field $B_0 = 0.5$ T, which is necessary to yield reliable information on the magnetic dipole orientation with respect to the local symmetry elements. CONDON takes into account the following single-ion effects: ligand-field effects (H_{lf}), interelectronic repulsion (H_{ee}), spin−orbit coupling (H_{so}), and the applied field (H_{mag}). Generally, for a magnetically isolated $3d^N$ metal ion in a ligand-field (lf) environment in an external magnetic field B, the Hamiltonian of the metal ion is represented by[31,32]

$$H = H_{\text{lf}} + H_{\text{ee}} + H_{\text{so}} + H_{\text{mag}}$$

which can be considered as an extension of the EHCF d-shell Hamiltonian on account of the spin−orbit interaction operator H_{so} and of the operator describing the interaction with the applied magnetic field H_{mag}. Figures 6 and 7 show the experimental magnetization (μ_{eff}, SI units; $\mu_{\text{eff}} = 797.74[\chi_m T]^{1/2}$) of **1** and **2** in the temperature range 2−300 K. This data set was fitted to the above-stated spin Hamiltonian using the ligand-field effect, spin−orbit coupling, and exchange coupling. The values for the spin−orbit coupling parameter ($\zeta = 600$ cm^{-1}[32]) and Racah parameters ($B = 783$ cm^{-1}, $C = 3687$ cm^{-1}[25]) were chosen on the basis of the optical spectra, consistent with our EHCF calculations. The exchange interactions between the metal centers are considered in the molecular field approximation

$$\chi_m^{-1} = \chi_m'^{-1}(B, C, \zeta, B_q^k) - \lambda_{\text{mf}}$$

where χ_m' represents the single-center susceptibility and λ_{mf} the molecular field parameter. The quantities B_q^k

(27) Eyert, V.; Siberchicot, B.; Verdaguer, M. *Phys. Rev. B* **1997**, *56*, 8959.
(28) Middlemiss, D. S.; Lawtonand, L. M.; Wilson, C. C. *J. Phys.: Condens. Matter* **2008**, *20*, 335231.
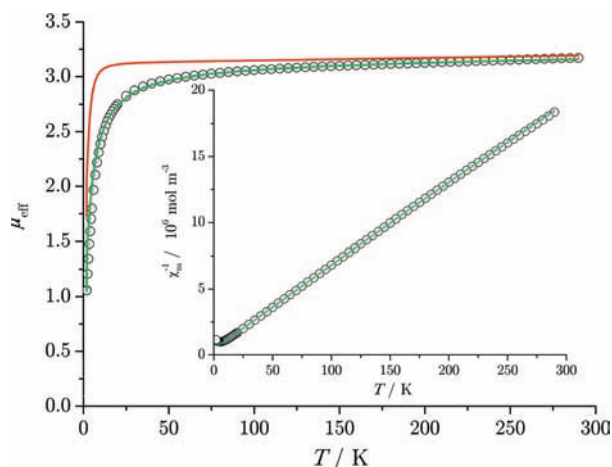(29) Nishino, M.; Yoshioka, Y.; Yamaguchi, K. *Chem. Phys. Lett.* **1998**, *297*, 51.

(30) Schilder, H.; Lueken, H. *J. Magn. Magn. Mater.* **2004**, *281*, 17.
(31) Wybourne, B. G. In *Spectroscopic Properties of Rare Earths*; Wiley: New York, 1965.
(32) Görller-Walrand, C.; Binnemans, K. In *Handbook on the Physics and Chemistry of Rare Earths*; Gschneidner, K. A., Jr., Eyring, L., Eds.; Elsevier: Amsterdam, 1996; Vol. *23*, Ch. 155, p 121.

Figure 6. Temperature-dependence of μ_{eff} of Ni(CN)$_2$RbCl (**1**) (circles) at an applied field of $B_0 = 0.5$ T (green line, least-squares fit; red line, single-ion effects).
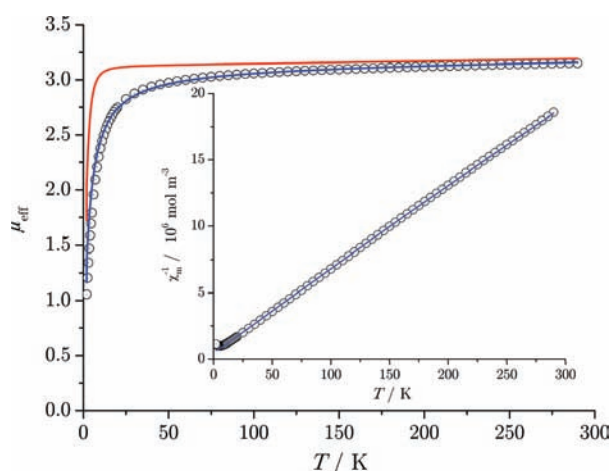
Figure 7. Temperature-dependence of μ_{eff} of Ni(CN)$_2$CsCl (**2**) (circles) at an applied field of $B_0 = 0.5$ T (blue line, least-squares fit; red line, single-ion effects), see text for parameters.

represent the crystal/ligand-field parameters in Wyborne notation (B_0^2, B_0^4, and B_4^4 for an enlongated octahedral coordination environment),[31] according to

$$H_{\text{lf}} = B_0^2 \sum_{i=1}^{N} C_0^2(i) + B_0^4 \sum_{i=1}^{N} C_0^4(i) + B_4^4 \sum_{i=1}^{N} (C_4^4(i) + C_{-4}^4(i))$$

where $C_q^k(i)$ are the Racah tensor components describing the angular dependence of the ligand field. The B_q^k parameters can be determined either by fitting experimental data (inverse spectral problem) or by the above EHCF procedure (direct spectral problem).

At room temperature, the effective Bohr magneton number is roughly 3.2 μ_{B} per Ni$_2$(CN)$_4$M$_2$X$_2$ unit, i.e., per hs Ni^{2+} center, a value that is larger than the spin-only value of 2.83 μ_{B}, and corresponds to the value 3.14 μ_{B} resulting from the EHCF $^3B_2 \rightarrow {}^1A_1$ transition energy and the above value of ζ according to eq 4.82 of ref 11 as well as with the expected μ_{eff} value in hs complexes in the range

(33) König, E.; Kremer, S. In *Magnetism Diagrams for Transition Metal Ions*; Plenum Press: New York, 1979; pp 305−320.

3.0−3.5 for dilute Ni^{2+} ($S = 1$) systems.[33] The μ_{eff} values of **1** and **2** slightly decrease with decreasing temperature in the range 100−300 K, as one could expect from eq 4.82 of ref 11, and a more pronounced decrease occurs below 100 K. This monotonous decrease of μ_{eff} toward lower temperatures could be attributed to both single-ion effects and antiferromagnetic interactions. The linear fit in the χ^{-1}_{m} vs T plot (Figures 6 and 7, insets) in the temperature range $T = 50{-}290$ K for compounds **1** and **2** yields a Weiss temperature $\theta_{\text{p}} \approx -6$ K, indicating overall weak AF coupling. For **1** and **2**, the fitting procedure employs starting values for the ligand-field parameters $B_0^2 = 2268$ cm^{-1}, $B_0^4 = 20118$ cm^{-1}, and $B_4^4 = 14696$ cm^{-1} that are directly derived from the calculated parameters Dq, Ds, and Dt [$-7Ds = B_0^2$; $B_0^4 = 21(Dq - Dt)$; $B_4^4 = 3(35/2)^{1/2}Dq$ (see ref 11)]. A best fit results for $B_0^2 = 2250$ cm^{-1}, $B_0^4 = 20200$ cm^{-1}, and $B_4^4 = 16900$ cm^{-1} for both **1** and **2**, which are in an almost ideal agreement with the EHCF values, and $\lambda_{\text{mf}} = -3.88 \times 10^5$ (**1**) and $\lambda_{\text{mf}} = -3.92 \times 10^5$ mol m^{-3} (**2**) ($SQ = 0.6\%$), indicating antiferromagnetic coupling. The red lines in Figures 6 and 7 illustrate the temperature dependence of μ_{eff} exclusively in terms of isolated single-ion effects in the absence of AF exchange coupling. Otherwise—with an account of antiferromagnetic interactions—the ligand field splitting derived from this magnetochemical analysis corresponds well to spectroscopic data on tetragonally distorted octahedral Ni^{2+} complexes[14,33] and is in line with our EHCF calculations.

Magneto-Structural Relations

Structural Issues. The structures of the MNi(CN)$_2$X phases are depicted in Figures 2−4. The Ni^{2+} ions, which are nearest to each given hs Ni^{2+} ion, are the ls ones and do not contribute to the magnetic response of the sample. Thus only the hs (nitrile-coordinated) neighbors of any hs Ni^{2+} ion must be taken into account when discussing the magnetic structure. Under these conditions, each hs Ni^{2+} ion has eight hs nearest neighbors in the same Ni(CN)$_2$ plane and eight more in the parallel planes. The hs neighbors of a hs Ni^{2+} ion in its own plane structurally fall into two subclasses: (1) those separated by a ls Ni^{2+} ion in the linear fashion as represented in Figure 3—in this case the hs Ni−hs Ni separation in **1** amounts to 10.06 Å—and (2) those situated on a similar parallel line, as can be seen in Figure 4. In the latter case, the intralayer hs-Ni/hs-Ni separation in **1** amounts to 7.11 Å. These values can be compared (3) with the hs-Ni/hs-Ni interlayer separation of 7.45 Å in **1**—Figure 2 (the structural interlayer distance in this material is 5.46 Å, but it corresponds to the hs-Ni/ls-Ni contact). At these characteristic distances between the hs Ni^{2+} ions, the direct exchange is not possible any more so that some kind of superexchange has to be responsible for the appearance of the molecular field λ_{mf}.

On the basis of the structural classification of the above nearest hs-Ni/hs-Ni pairs of the types 1−3, one can expect three values of the effective exchange parameters: $J^{(1)}$ for the linear arrangement, $J^{(2)}$ for the intralayer interline arrangement, and $J^{(3)}$ for the interlayer arrangement. This has been depicted in Figure 8.
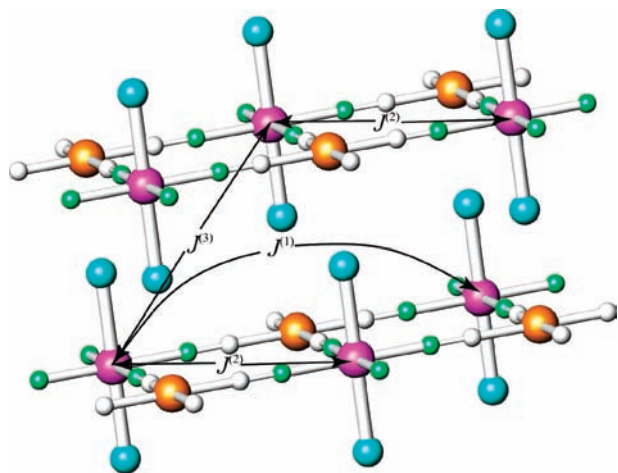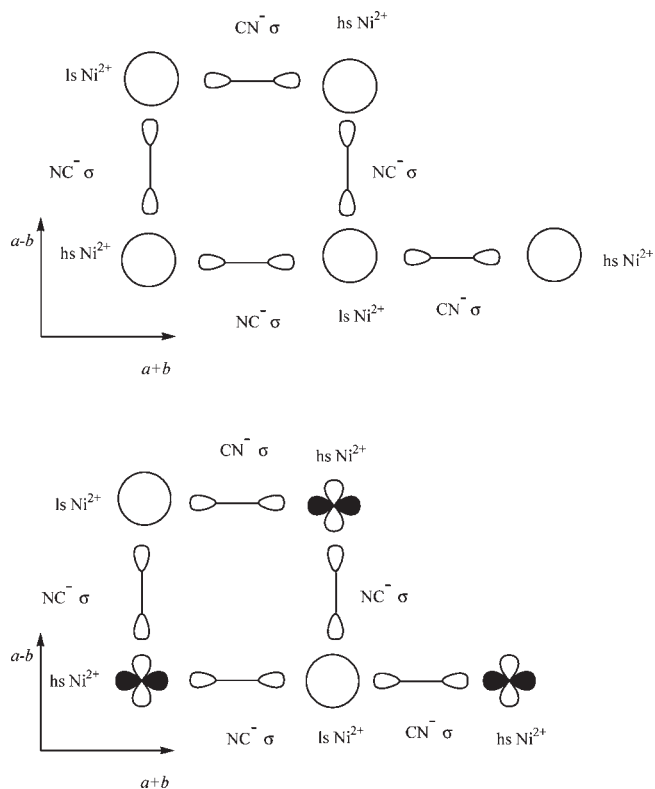
Figure 8. Representative examples of the pairs of hs Ni^{2+} ions coupled by the exchange interactions $J^{(1)}$, $J^{(2)}$, and $J^{(3)}$. Color code as before.

Superexchange Paths and Exchange Parameters. Following refs 34 and 35, the superexchange paths are controlled by the overlaps of the magnetic ions with those of the diamagnetic constituents. The (antiferromagnetic) superexchange path then appears when the magnetic orbitals residing in different magnetic ions can be connected by a sequence of the overlapping orbitals, which may bring the magnetic electrons residing in different magnetic ions into contact by a sequence of the electron or hole hops through, respectively, empty or filled orbitals of the magnetically silent components.

Let us consider characteristic overlaps of the magnetic and tentative intermediate orbitals. On the basis of the EHCF analysis, it has been concluded that the magnetic electrons in the hs Ni^{2+} centers occupy the a_1 and b_2 orbitals (d_{z^2} and d_{xy}). The magnetic a_1 and b_2 orbitals do not overlap with either π orbitals of the CN units—neither those of π symmetry with respect to the $Ni(CN)_2$ planes nor those lying in these planes—but possess π symmetry only with respect to the Ni−NC/CN axes. Thus, the π orbitals of the CN units can be safely excluded from the consideration as possible superexchange mediators. This is fairly different from other magnets of the Prussian blue family reported so far where the CN π orbitals played a dominant role in the superexchange mediation.[29,36,37] Analogously, the Cl^- orbitals of π symmetry with respect to the Ni−Cl−Ni axes (p_x and p_y ones) do not overlap with either a_1 or b_2 magnetic orbitals since the former is of σ and the latter of δ symmetry with respect to this axis. Thus, the Cl^- π orbitals cannot mediate any antiferromagnetic superexchange either. By contrast, the magnetic a_1 and b_2 orbitals of the hs Ni^{2+} ions overlap both with the occupied σ and empty σ^* orbitals of the CN^- anions and with the occupied Cl^- p_z orbitals having σ symmetry with respect to the Ni−Cl−Ni axes. The b_2 orbitals of the hs Ni^{2+} ions cannot take part in the interlayer superexchange since

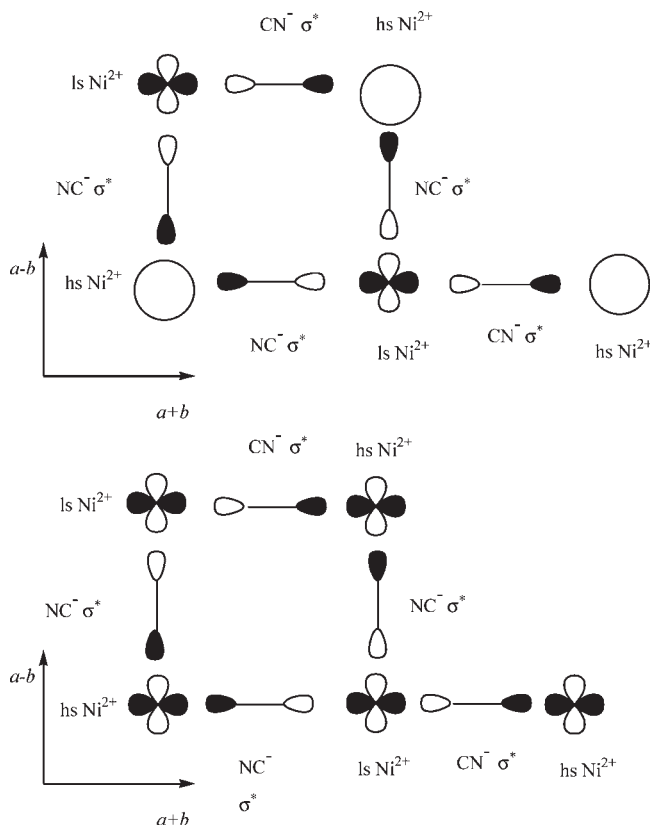(34) Goodenough, J. B. *Magnetism and the Chemical Bond*; Interscience-Wiley: New York, 1963.
(35) Kahn, O. *Molecular Magnetism*; VCH: New York, 1993.
(36) Nishino, M.; Yoshioka, Y.; Yamaguchi, K. *Chem. Phys. Lett.* **1998**, *297*, 51.
(37) Atanasov, M.; Comba, P.; Daul, C. A. *J. Phys. Chem. A* **2006**, *110*, 13332.

Figure 9. The occupied orbitals of the CN^- and ls Ni^{2+} ions involved in the hole propagation yielding intralayer superexchange paths for the antiferromagnetic coupling of the local momenta residing in the hs Ni^{2+} ions. a_1 (top) and b_2 (below) magnetic orbitals seen along the c axis.

they do not overlap with the occupied Cl^- p_z orbitals so that only the a_1 orbitals need to be considered. The overlaps just mentioned can lead, however, only from a hs Ni^{2+} ion to a neighboring ls Ni^{2+} ion, rather than to other hs Ni^{2+} ions. However, involvement of the magnetically silent ($S = 0$) transition metal ions in the superexchange paths has been proposed, e.g., in ref 38. These species can mediate the superexchange in the same way, as do other magnetically silent species. The only significant difference comes from the different symmetry of the involved intermediate d orbitals on the ls Ni^{2+} centers, which results in unexpected (from the point of view of the standard Goodenough−Kanamori rules) directions of the superexchange. It seems to be relevant to consider the same a_1 and b_2 orbitals, which are, however, doubly occupied and empty, respectively, in the ls Ni^{2+} ions.

In Figures 9−11, the overlaps of the magnetic and nonmagnetic orbitals have been sketched. The involvement of the a_1 and b_2 orbitals of the ls Ni^{2+} ions makes angular antiferromagnetic superexchange possible. The individual paths involve the same intermediate states and equal individual hopping parameters corresponding to each one-electron/one-hole transfer through each overlap. Thus, the angular and linear superexchange paths equally contribute to the respective effective exchange parameters $J^{(1)}$ and $J^{(2)}$. For the pair of interacting hs Ni^{2+} ions in the angular arrangement, there are two equivalent superexchange paths (one with the ls Ni^{2+} in the upper left corner and another one with the ls

(38) Papanikolaou, D.; Kosaka, W.; Margadonna, S.; Kagi, H.; Ohkoshi, S.; Prassides, K. *J. Phys. Chem. C* **2007**, *111*, 8086.

Figure 10. The empty orbitals of the CN^- and ls Ni^{2+} ions involved in the electron propagation yielding intralayer superexchange paths for the antiferromagnetic coupling of the local momenta residing in the hs Ni^{2+} ions. a_1 (top) and b_2 (below) magnetic orbitals seen along the c axis.
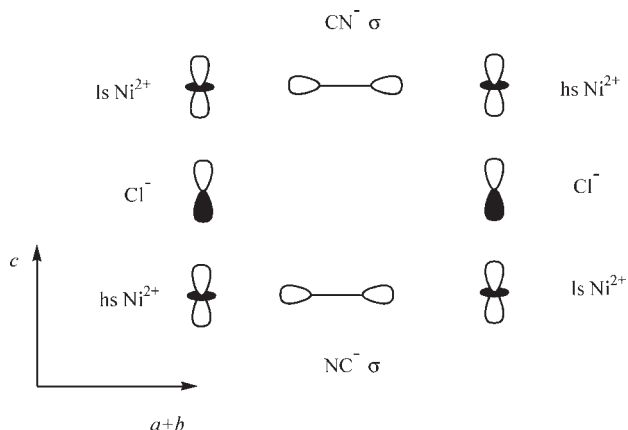
Figure 11. The occupied orbitals of the CN^-, Cl^-, and ls Ni^{2+} involved in hole propagation, yielding interlayer superexchange paths for antiferromagnetic coupling between local momenta residing in the hs Ni^{2+} ions through the occupied Cl^- p_z states and the a_1 orbitals of the ls Ni^{2+} ions (view perpendicular to the c axis). The b_2 orbitals of Ni^{2+} ions (either hs or ls) are not involved for symmetry reasons. As in Figure 10, two paths going through the ls Ni^{2+}, Cl^-, and CN^- ions equally contribute to the exchange parameter $J^{(3)}$ of different layers, as shown in Figures 2 and 8.

Ni^{2+} ion on the horizontal path), whereas for the linear arrangement of two neighboring hs Ni^{2+} ions, there is only one such superexchange path (horizontal). Thus, we estimate the effective *intra*layer exchange parameters as $J^{(2)} \approx 2J^{(1)} = J_\parallel$. Similarly, one can estimate the *inter*layer effective exchange $J^{(3)} = J_\perp$ to be on the same order of magnitude as $J^{(2)}$ (Figure 11). The fact that, for symmetry

reasons, only the a_1 holes can propagate through the occupied Cl^- p_z orbitals further scales down this effective exchange so that we can write $J_\perp = \alpha J_\parallel$, $0 < \alpha < 1$.

Magnetic Structure and Estimates of Characteristic Temperatures. Taking into account the number of neighbors of the different types listed above, we obtain, using formula eq 5.46 of ref 10, see also eq 22.104 of ref 39, the Weiss temperature:

$$|\theta_\mathrm{p}| = \frac{4}{3k_\mathrm{B}}(6 + 8\alpha)J_\parallel$$

With this estimate, we try to figure out possible magnetically ordered ground states. Because the dominating effective exchange parameter is that along the intralayer angular superexchange path ($J^{(2)}$), the spins coupled by those superexchange paths must be antiparallel in the antiferromagnetic ground state (which is assumed in order to conform with the sign of the experimental λ_mf parameters). In this case, the momenta residing on the hs Ni^{2+} ions along the straight lines shown in Figures 3 and 4 must be aligned in the same direction, thus producing a certain amount of frustration not expected on purely geometric grounds. Due to smaller effective exchange coupling in such ion pairs ($J^{(1)}$) this possibly does not destroy the overall antiferromagnetic order in the layers but reduces the ordering (Néel) temperature of the latter[39] since these interactions must be accounted for with the opposite sign. This particular spin arrangement is depicted in Figure 12. Analogously, only half of the momenta of eight hs Ni^{2+} neighbor ions lying in the parallel layers and coupled through the Cl^- ions align antiparallel to a given one; the other half of the momenta align parallel to the momentum of the given hs ion. Thus, in the molecular-field approximation, the contribution of the interlayer interactions to the Néel temperature vanishes. This is shown in Figure 13 representing the overall magnetic structure of the $MNi(CN)_2X$ phases.

Finally, the relevant estimates (see ref 39, eqs 22.108 and 22.110) read

$$\theta_\mathrm{N} = \frac{4}{3k_\mathrm{B}}2J_\parallel$$

$$\frac{\theta_\mathrm{N}}{|\theta_\mathrm{p}|} = \frac{1}{(3 + 4\alpha)}$$

which yields the upper bound of the Néel temperature to be $\theta_\mathrm{N} < 2\,\mathrm{K}$, which is slightly lower than the lower border of the magnetic measurements performed so far.

The magnitude of the effective exchange thus estimated is much smaller than one would expect on the basis of the experimental and theoretical data collected and calculated in ref 40 for the nickel-containing Prussian blue analogs. These suggested the critical temperature of the respective magnetic transitions to be on the order of several tens of Kelvin. The reason for this difference is that those so far reported Prussian blue analogs containing Ni were only those where the Ni^{2+} ions occured in the

(39) Vonsovskii, S. V. *Magnetism*; Nauka: Moscow, 1971 [in Russian]. Vonsovsky, S. V. *Magnetism*: Wiley: New York, 1974 in two volumes.
(40) Ruiz, E.; Rodriguez-Fortea, A.; Alvarez, S.; Verdaguer, M. *Chem.—Eur. J.* **2005**, *11*, 2135.
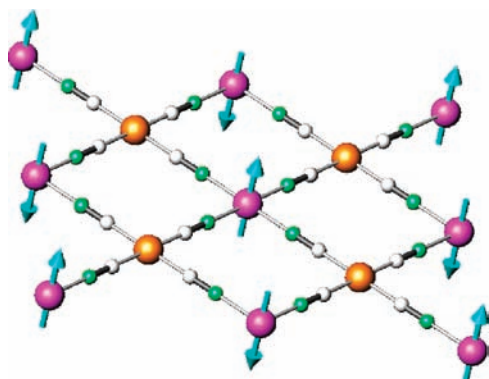
Figure 12. Tentative magnetic structure of the $Ni(CN)_2$ layer in the $Ni(CN)_2MX$ material. Arrows indicate the direction of local magnetic momenta residing on the hs Ni^{2+} ions; color code as before.
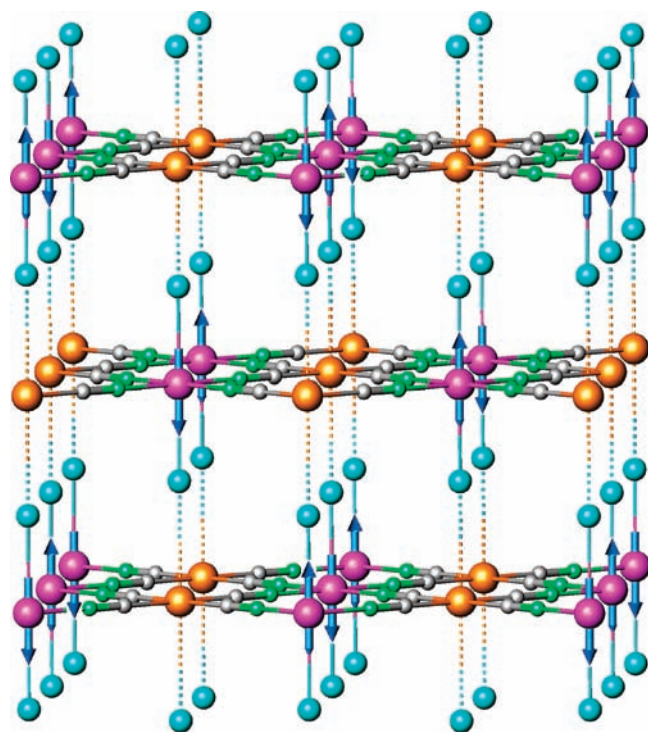
Figure 13. Tentative three-dimensional magnetic structure of the Ni-$(CN)_2MX$ material. Arrows indicate the direction of local magnetic momenta residing on the hs Ni^{2+} ions; color code as before.

nitrile coordination (hs) and were immediately coupled to the next magnetic ion through only one NC bridge. By

contrast, in the present series of compounds, half of the Ni^{2+} ions occur in the cyanide type of coordination, which results in the ls (magnetically silent) ions. These units have been suggested in ref 41 to be capable of mediating pretty weak ferromagnetic exchange (on the order of a few Kelvin) between the hs Ni^{2+} ions coordinated by a macrocyclic amine. On the other hand, unlike another tetracyano magnetic component/bridge ([Mn^{IV}-$(CN)_4]^{2-}$) which is reported to be tetrahedral in 42, either the $[Ni(CN)_4]^{2-}$ or the $[Ni(NC)_4]^{2-}$ are perfectly planar.

Conclusion

We have reported the synthesis of four new two-dimensional Ni-based analogs of Prussian blue, characterized by X-ray crystallography as well as optical and magnetic measurements. The crystal structures resemble a distorted perovskite type and comprise elongated $[Ni(NC)_4X_2]^{4-}$ and $[Ni(CN)_4X_2]^{4-}$ octahedra, which are charge-balanced by M^+ cations located in the voids. The electronic structure of the new family of materials was studied by the GGA+U and EHCF methods. Both consistently suggest the presence of hs ($S = 1$) and ls ($S = 0$) Ni^{2+} ions prescribed by the structurally found purely nitrile or cyanide coordination pattern, in line with the optical (UV–vis) study. The magnetic measurements corroborate the calculated electronic structure: the temperature dependence of the effective magnetic momentum conforms to the presence of both hs and ls Ni^{2+} ions in a 1:1 proportion with weak overall antiferromagnetic coupling between the hs ions. The ligand-field parameters as extracted from the temperature-dependent effective magnetic moment fairly agree with the spectral data and the EHCF estimates. The final picture of the effective magnetic exchange interactions includes linear and angular intralayer and interlayer antiferromagnetic superexchange paths, which connect fairly distant magnetic ions with structurally different mutual positions. Estimates of the relative magnitudes of the exchange parameters are made on the basis of the analysis of the superexchange paths. The Néel-style ground state still conforms with the available experimental estimates of the Weiss and Néel temperatures.

(41) Kou, H.-Z.; Si, S.-F.; Gao, S.; Liao, D.-Z.; Jiang, Z.-H.; Yan, S.-P.; Fan, Y.-G.; Wang, G.-L. *Eur. J. Inorg. Chem.* **2002**, 699.

(42) Miller, J. S.; Manson, J. L. *Acc. Chem. Res.* **2001**, *34*, 563.